Ceramics International 47 (2021) 11052–11062

Contents lists available at ScienceDirect

Ceramics International

journal homepage: www.elsevier.com/locate/ceramint

Exploring the tribological behavior of Ti/Al-DLC/PAO/graphene oxide nanocomposite system

Xiaowei Xu [a,c], Peng Guo [a], Xiaowei Li [a,b,d,*], Kwang-Ryeol Lee [d], Ping Cui [a,c], Aiying Wang [a,e,f,**]

[a] Key Laboratory of Marine Materials and Related Technologies, Zhejiang Key Laboratory of Marine Materials and Protective Technologies, Ningbo Institute of Materials Technology and Engineering, Chinese Academy of Sciences, Ningbo, 315201, PR China
[b] School of Materials and Physics, China University of Mining and Technology, Xuzhou, 221116, PR China
[c] School of Physical Science and Technology, ShanghaiTech University, Shanghai, 201210, PR China
[d] Computational Science Center, Korea Institute of Science and Technology, Seoul, 136-791, Republic of Korea
[e] Ningbo Institute of Industrial Technology, Chinese Academy of Sciences, PR China
[f] Center of Materials Science and Optoelectronics Engineering, University of Chinese Academy of Sciences, Beijing, 100049, PR China

ARTICLE INFO

Keywords:
Diamond-like carbon
Graphene oxide
Lubrication mechanism
Tribological property

ABSTRACT

The role of graphene oxide (GO) as an oil-based additive on the tribological behavior of Ti/Al-DLC films and its dependence on GO concentration were systematically investigated. The results revealed that, compared to the additive-free case, the system with a GO concentration of 0.003 wt% achieved remarkable friction reduction and wear resistance, which were decreased by 38.4% and 23.5%, respectively. This is attributed to the synergistic effect of tribo-induced graphitization and the adsorption of GO on the worn surface. However, when the GO concentration was further increased, it induced the clumping of the GO additive, causing increased friction coefficient and severe abrasive wear of the worn surface.

1. Introduction

In modern industry, the moving assemblies used in aerospace, aviation, military, and other engineering fields are inevitably subject to friction and wear, resulting in energy dissipation and material losses [1–4]. Therefore, it is important to minimize friction and reduce wear, thus improving machine efficiency. However, owing to the complex and changeable working environment, single-liquid lubricants cannot satisfy the rigorous requirement of mechanical components for reducing friction and extending the machine service lifetime. Many previous studies [5–8] have confirmed the solid–liquid lubricating system, which combines solid lubricating films/coatings with fluid lubricants to be an effective method of reducing friction. In comparison with the traditional hard anti-wear coating and soft lubricating protective coating, a diamond-like carbon (DLC) film, exhibits superior comprehensive performance as a high-performance solid lubricating film [9–11]. In particular, co-doping with binary metals into DLC film can further endow the film with enhanced mechanical and tribological performances [12–15].

As oil-based lubricant additives for liquid lubricants, graphene and its derivatives have attracted attention because of their ultrathin 2D laminated structure, superior load-bearing capacity, as well as excellent friction reduction and anti-wear capabilities [16–18]. Zhang et al. [19] reported that the lubricating oil with oleic acid-modified graphene (0.02.0.06 wt%) exhibited 17% and 14% reduction in friction coefficient (COF) and wear scar diameter (WSD), respectively. Eswaraiah et al. [20] reported a type of engine lubricant oil with a graphene nanoadditive which showed a decrease of 80% in COF and a decrease of over 30% in wear rate. Similarly, Wu et al. [21] evaluated the tribological behavior of Si_3N_4 ceramic/GCr15 sliding pairs lubricated by 4010 AL base oil containing graphene oxide (GO) nanosheets and found that as the GO concentration was 0.5 wt%, the tribopairs exhibited excellent antifriction and wear-resistant properties owing to the formation of a protective tribofilm, which adhered to the worn surface to prevent the direct contact of tribopairs. Moreover, Zhang et al. [22] illustrated that multilayer GO, which functions as a Mobil DTE oil additive, can reduce

* Corresponding author. Key Laboratory of Marine Materials and Related Technologies, Zhejiang Key Laboratory of Marine Materials and Protective Technologies, Ningbo Institute of Materials Technology and Engineering, Chinese Academy of Sciences, Ningbo, 315201, PR China.
** Corresponding author. Key Laboratory of Marine Materials and Related Technologies, Zhejiang Key Laboratory of Marine Materials and Protective Technologies, Ningbo Institute of Materials Technology and Engineering, Chinese Academy of Sciences, Ningbo, 315201, PR China.
E-mail addresses: lixw0826@gmail.com (X. Li), aywang@nimte.ac.cn (A. Wang).

https://doi.org/10.1016/j.ceramint.2020.12.228
Received 3 October 2020; Received in revised form 13 December 2020; Accepted 21 December 2020
Available online 27 December 2020

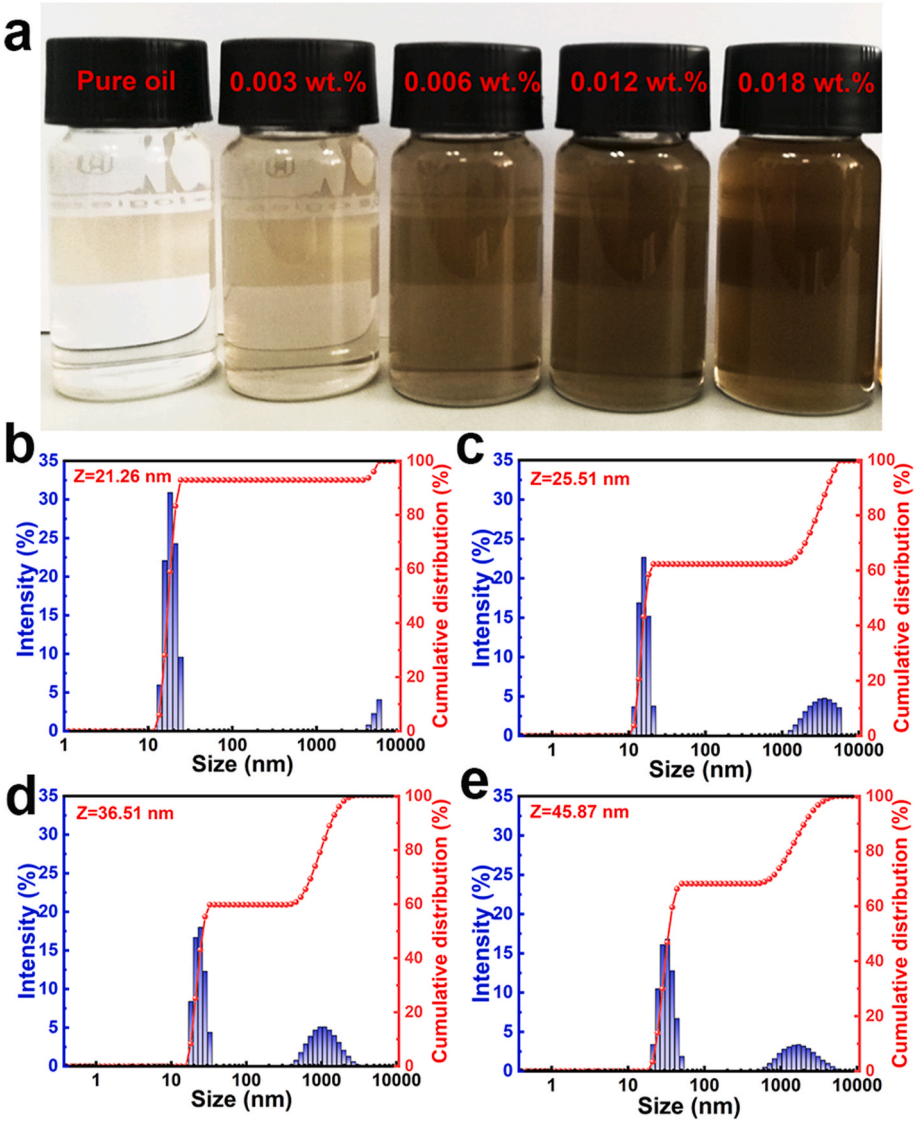

Fig. 1. (a) Digital photographs of GO-dispersed PAO oils with different GO concentrations after aging for 5 h. Laser particle-size distributions of (b) PAO-GO1, (c) PAO-GO2, (d) PAO-GO3, and (e) PAO-GO4 oils.

the average COF by 67.37%.

Although a considerable number of studies have been focused on the tribological properties of steel/steel or ceramic/steel pairs lubricated with graphene and its derivatives as oil-based additives, the effects of graphene-based additives on metal-doped DLC/steel pairs remain unclear. In previous studies [23–26], we have fabricated the Ti/Al co-doped DLC (Ti/Al-DLC) film using a hybrid ion beam (HIB) deposition system, which showed superior antifriction and wear-resistant behavior under dry conditions. Therefore, in the present work, we further evaluate the tribological behavior of Ti/Al-DLC film composited with poly-alpha olefin (PAO) as the base oil and GO as the additive. We focused on its dependence on the GO concentration and discussed the underlying friction mechanism with respect to the structural analysis of the friction interface.

2. Experimental details

2.1. Liquid lubricant

The liquid lubricant consisted of PAO oil as the base oil and GO as the lubricant additive; high-purity GO was purchased from Nanjing Jicang Nano Technology Co., Ltd., and its thickness was approximately 1–2 nm. The PAO oil, provided by Shell China Ltd (Shanghai), was mainly composed of hydrocarbons. To prepare the blended lubricants, GO powder was first added to the PAO-based oil and then subjected to ultrasonic dispersion for 180 min. The GO concentration ranged from 0 wt %, 0.003 wt%, 0.006 wt%, 0.012 wt%, to 0.018 wt%, and the corresponding lubricants were abbreviated as Pure oil, PAO-GO1, PAO-GO2, PAO-GO3, and PAO-GO4, respectively.

2.2. Film deposition

Ti/Al-DLC films were deposited on a silicon P (100) wafer using the HIB technique, which was composed of a linear anode-layer ion source (ALIS) supplied with C_2H_2 gas for DLC deposition and a direct current magnetron sputtering (DCMS) device provided with a $Ti_{50}Al_{50}$ (99.99%) target. Prior to deposition, the substrates were ultrasonically cleaned in ethyl alcohol and then etched in Ar^+ bombardment for 20 min to remove the adhered contamination. During deposition, a Ti/Al interlayer was first deposited on the substrate under conditions of 55 sccm Ar, a sputtering current of 4 A, bias voltage of −100 V, and deposition time of 16 min [25]. After that, 70 sccm Ar and 10 sccm C_2H_2 were supplied to

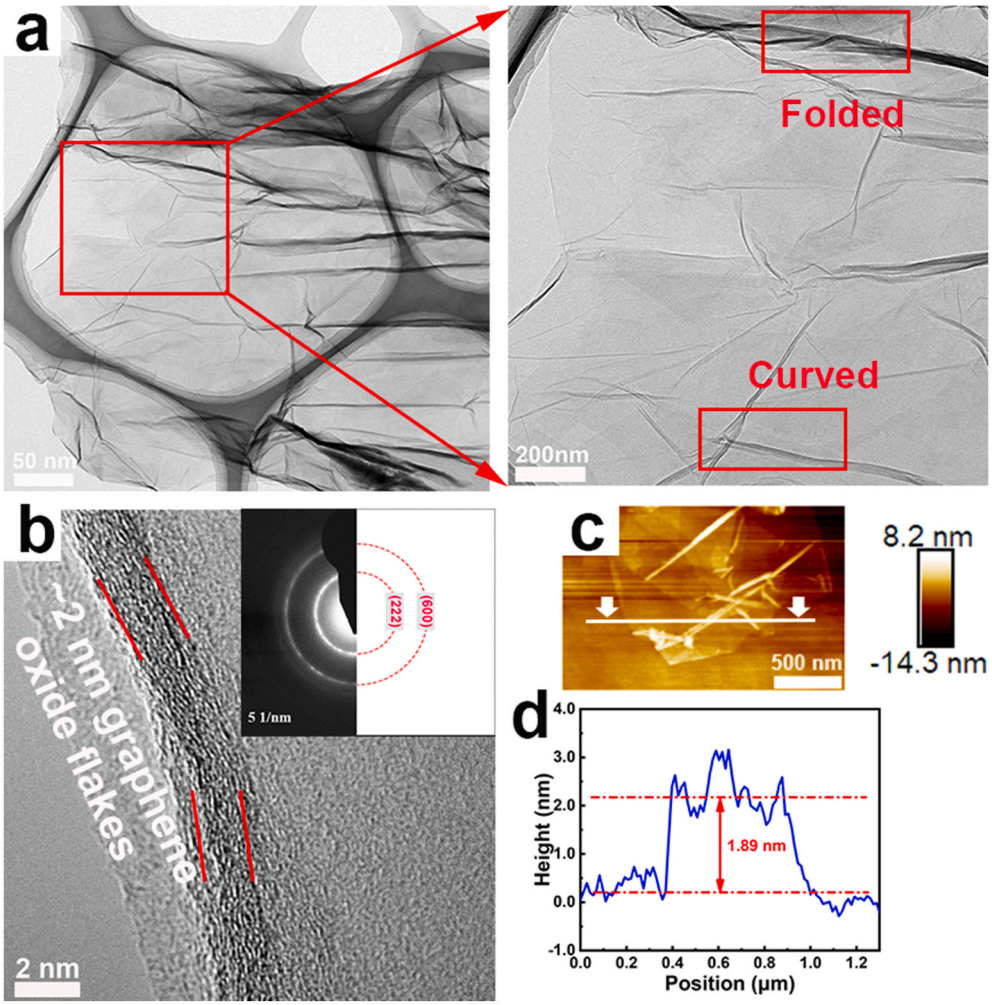

Fig. 2. (a) TEM micrographs, (b) HR-TEM lattice plane and corresponding SAED diagram of GO, (c) AFM image, and (d) corresponding cross-sectional profile of 2D AFM image of as-prepared GO additive.

DCMS and ALIS simultaneously to deposit the Ti/Al-DLC film; the ALIS current, sputtering current, negative-bias voltage, and deposition time were 0.2 A, 2.5 A, −50 V, and 60 min, respectively. Details of the deposition parameters can be obtained in our previous studies [23,27].

2.3. Microstructure characterization

The chemical structures of GO, PAO, and PAO-GO were characterized using Fourier transform infrared spectra (FTIR, NICOLET 6700) with the wave number ranging from 400 to 4000 cm^{-1}. The morphology and thickness of GO nanoplates were obtained by the high-resolution transmission electron microscopy (FEI Tecnai F20) and scanning probe microscope (Veeco Dimension 3100 V, SPM). The particle-size distribution of each oil sample was tested by the dynamic light scattering particle size analyzer (Zetasizer Nano ZS, ZETA). Furthermore, the profile of wear tracks was recorded using a surface profilometer (Alpha-step IQ, US) through a linear scanning mode. The field emission scanning electron microscopy (SEM, FEI Quanta FEG 250) combined with the X-ray energy dispersive spectroscopy (EDS) was utilized to analyze the surface morphologies of wear scar on the contact ball and the wear track on the film, respectively. The carbon bond structure of wear track was also investigated by Raman spectroscopy (Renishaw, inVia-reflex) with the laser wavelength of 532 nm.

2.4. Tribological testing

The tribological properties of the Ti/Al-DLC/PAO/GO composite system were evaluated using a pin-on-disk tribometer (Anton Paar, TRB3) at room temperature (20 ± 5 °C). A grinding GCr15 steel ball (HRC60) with a diameter of 6 mm was selected as the mating material. Each test was undertaken at a rotating speed of 320 rpm, an applied load of 5 N, a radius of 1.5 mm, and sliding distance of 4500 laps. In addition, each sample test was repeated thrice to calculate the average COF (μ) and wear rate (W). After the tests, the surfaces of the counterpart and film were ultrasonically cleaned with acetone. The wear rate of each sample was calculated using the Archard equation:

$$W = V / (L \times N) \tag{1}$$

where L and N were the total sliding distance and normal load separately; V corresponded to the wear-induced volume loss, which was calculated by the integral of cross-sectional profile of wear track. While the wear rate of mating ball was calculated as follows [28]:

$$V = \left(\frac{\pi h}{6}\right)\left(\frac{3D^2}{4} + h^2\right), \tag{2}$$

$$h = R - \sqrt{R^2 - \frac{D^2}{4}}, \tag{3}$$

where h was the height of wear material of the grinding ball; D and R

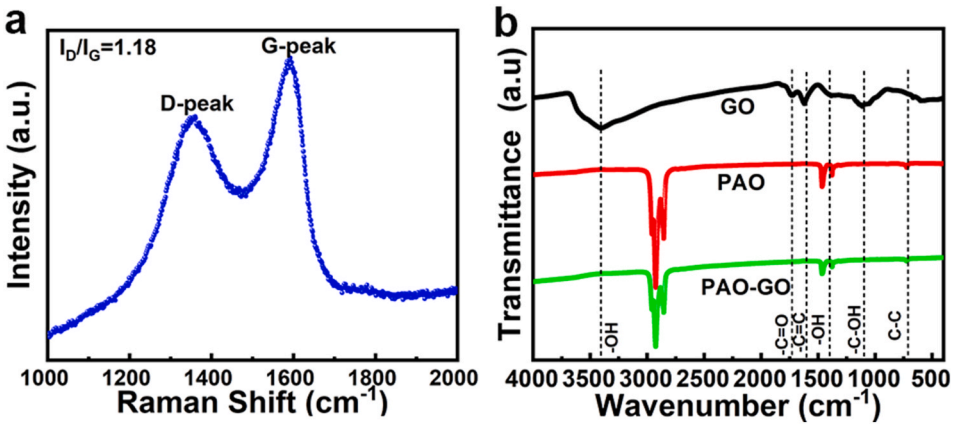

Fig. 3. (a) Raman spectrum of as-prepared GO; (b) FTIR spectra of GO, PAO, and PAO-GO, respectively.

were the diameter of wear scar and the radius of mating ball, respectively.

3. Results and discussion

3.1. Stability of GO-dispersed oil

GO-containing oil was prepared through a physical method without any extra dispersing agent. In order to confirm the stability of GO in PAO oil, Fig. 1(a) depicts the digital photographs of all GO-dispersed PAO oils with different GO concentrations after aging for 5 h. For comparison, pure PAO oil is also provided. Notably, there is no obvious sedimentation and separation of each observed oil sample, illustrating that the GO exhibits good dispersity and stability in the PAO oil. Fig. 1(b)–1(e) further display the laser particle-size distribution of each sample. It can be seen that as the GO concentration increases from 0.003 wt% to 0.018 wt%, the average particle size of GO increases from 21.26 to 45.87 nm. On the one hand, this proves that the GO can still remain at nanoscale sizes and good dispersion in PAO oil. On the other hand, the wide-laser particle-size distribution of GO indicates that GO mainly presents a particle-aggregation state rather than a monodisperse state in PAO-based lubricant oil.

3.2. Structure and morphology of GO additive

Fig. 2 demonstrates the structure and morphology of as-prepared GO. In Fig. 2(a), numerous wrinkles and curls exist in the GO nanoplates, which are mainly related to the degree of oxidation of GO and the surface energy [29], suggesting the existence of structural defects. The HRTEM lattice micrograph and corresponding selected area electron diffraction (SAED) diagram of GO are depicted in Fig. 2(b). Notably, the thickness of the GO nanoplates is approximately 2 nm, indicating the multilayer structure of GO [30]. In addition, the sharp crystalline diffraction rings are identified as (222) and (600) reflections of GO. Fig. 2(c) and (d) show the AFM morphology and cross-sectional profile, in which the white horizontal line is illustrated in 2D AFM morphology. It can be seen that the average thickness of GO comes out to be 1.89 nm, which is consistent with the TEM result.

Fig. 3(a) shows the Raman spectra of GO additive with a wavelength range of 1000–2000 cm^{-1}. It can be fitted into two prominent peaks: one is the D band at 1359 cm^{-1} corresponding to disordered sp^3-C caused by the structural defects of GO; the other is the G band located at 1591 cm^{-1}, which is associated with the in-plane vibration [31]. In addition, the intensity ratio of D peak to G peak (I_D/I_G) is closely related to the disorder degree of graphite materials [22,32]. In this case, the I_D/I_G ratio in GO is approximately 1.18, implying the structural defects of GO caused by the oxidation of functional groups. This is consistent with the TEM analysis. To further explore the structure of the functional group in GO and its interaction with PAO oil molecules, the FT-IR characterization is conducted, as shown in Fig. 3(b). For the GO, the absorption bands located at 1105 cm^{-1} and 1733 cm^{-1} are assigned to C–OH and C═O stretching vibrations of hydroxyl and carboxyl groups, respectively; the band at 1625 cm^{-1} is attributed to the unoxidized sp^2 C═C stretching vibration, whereas the bands at 3415 cm^{-1} and 1397 cm^{-1} originate from the stretching and bending vibrations of –OH, respectively [33]. For the pure PAO oil, the strong absorption bands in the region of 2855 cm^{-1} to 2970 cm^{-1} correspond to the stretching vibration of –CH_2 in alkyl chains; the bands at 1360 cm^{-1} and 1466 cm^{-1} are related to the vibrations of C–H group in PAO oil molecules [34–36]. After dispersing GO in PAO oil, each sample also shows the same peaks

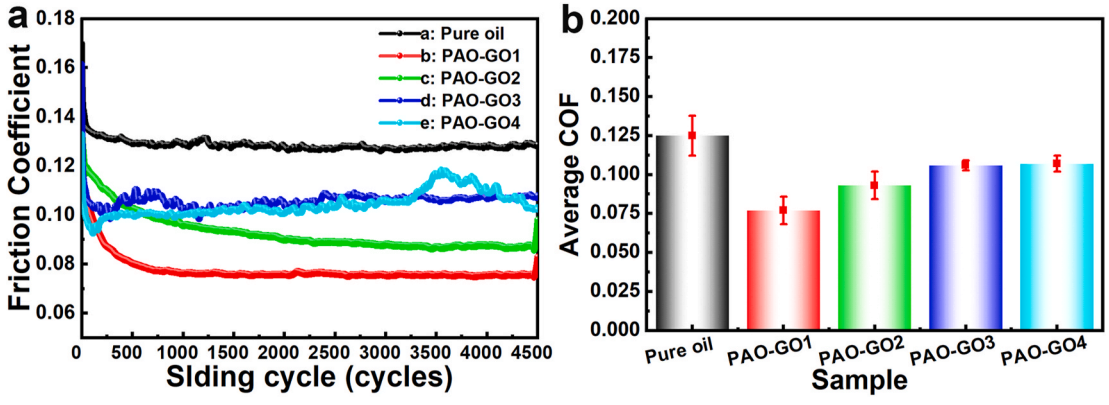

Fig. 4. (a) Friction curves and (b) average COF values of Ti/Al-DLC films lubricated by pure and GO-dispersed PAO oils, respectively.

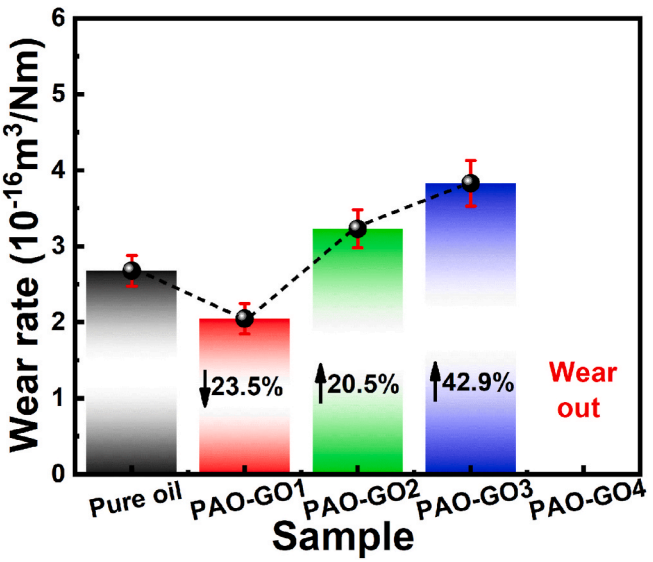

Fig. 5. Wear rates of Ti/Al-DLC films lubricated by pure and GO-dispersed PAO oils, respectively.

as those in pure PAO oil; however, no absorption peaks of GO can be observed. This phenomenon occurs mainly because when the graphene oxide content is low, the stretching vibration of $-CH_2$ in alkyl chains of the PAO oil has a strong absorption peak (Fig. 3(b)), which shows a shielding effect on the characteristic peaks of graphene oxide.

3.3. Tribological performance of Ti/Al-DLC/PAO/GO system

Fig. 4(a) displays the characteristic friction curves of the system lubricated by pure or GO-dispersed PAO oils. From the figure, compared to pure PAO, adding GO additive into oil could further reduce the COF value, suggesting the positive role of GO additive in the friction-reducing capacity of PAO oil. Furthermore, this change is strongly sensitive to the GO concentration. The average COF during the steady-state friction stage was calculated for each case, as illustrated in Fig. 4 (b). Compared to the pure PAO oil (0.125), when the concentration of GO additive in PAO oil is 0.003 wt%, the minimal COF value of 0.077 is obtained, which is reduced by 38.4%. However, with further increase in the GO concentration to 0.018 wt%, the COF values increases gradually, but it remains lower than that of the pure PAO oil, confirming the synergistic effect of GO additive and PAO oil. Meanwhile, the system with PAO-GO4 undergoes a long running-in process following an acute fluctuation owing to serious interaction between the GO sheets during the sliding process, as will be discussed later.

The wear rates of Ti/Al-DLC film lubricated by pure or GO-dispersed oils are given in Fig. 5. As can be seen that following the increase of GO concentration, the wear rate of composite system first shows a decreasing and then increasing trend, which coincides with the change of COF in Fig. 4(b). When the concentration of GO additive reached 0.003 wt% (PAO-GO1), the system exhibits a superior antiwear behavior and the wear rate is only approximately 2.05×10^{-16} m^3/Nm, which is approximately 23.5% lower than that lubricated by pure PAO oil. As the concentration of GO additive further increase to 0.006 wt% and 0.012 wt%, the wear rate conversely increases by 20.5% and 42.9%, respectively. However, when the concentration of GO additive was 0.018 wt% (PAO-GO4), the wear rate could not be calculated owing to the partial exfoliation of the Ti/Al-DLC film.

Moreover, the wear scars on each mating ball were analyzed, including the SEM image of the wear scar for each case and the corresponding WSD and wear rate, as illustrated in Figs. 6 and 7, respectively. Under the pure PAO oil, the wear scar on the steel ball is almost round in shape, and there exist some wide and deep scratches (Fig. 6(a)), indicating that abrasive wear occurs during the rubbing process. Compared with Fig. 6(a), the wear scar lubricated by PAO-GO1 shows a smaller wear scar (Fig. 6(b)) and a smoother worn surface (Fig. 7(a)). The wear rate of the mating ball also reaches the lowest value of 1.16×10^{-5}mm^{-3} (Fig. 7(b)), suggesting that excellent wear resistance was achieved when the GO concentration was 0.003 wt%. However, the WSD and wear rate of counterparts display continuously increasing

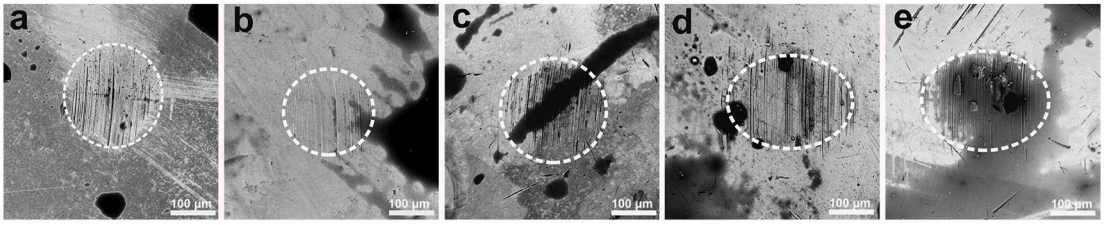

Fig. 6. SEM morphologies of wear scars on the mating balls lubricated by (a) pure PAO oil, (b) PAO-GO1, (c) PAO-GO2, (d) PAO-GO3, and (e) PAO-GO4, respectively.

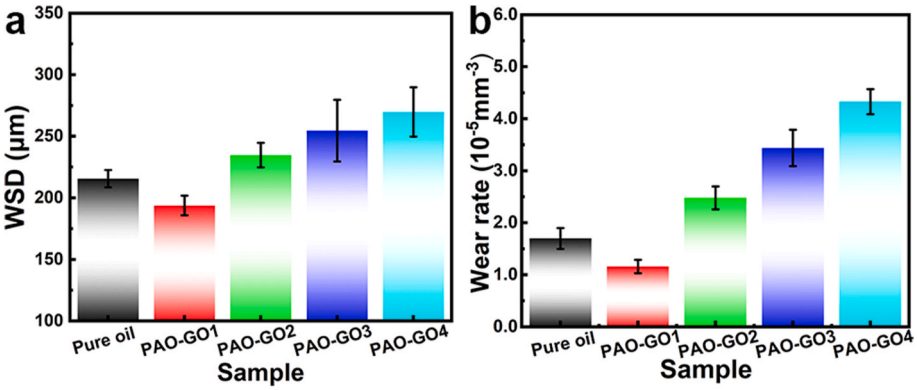

Fig. 7. (a) WSD and (b) wear rate of the mating balls lubricated by pure PAO oil and GO-dispersed oil, respectively.

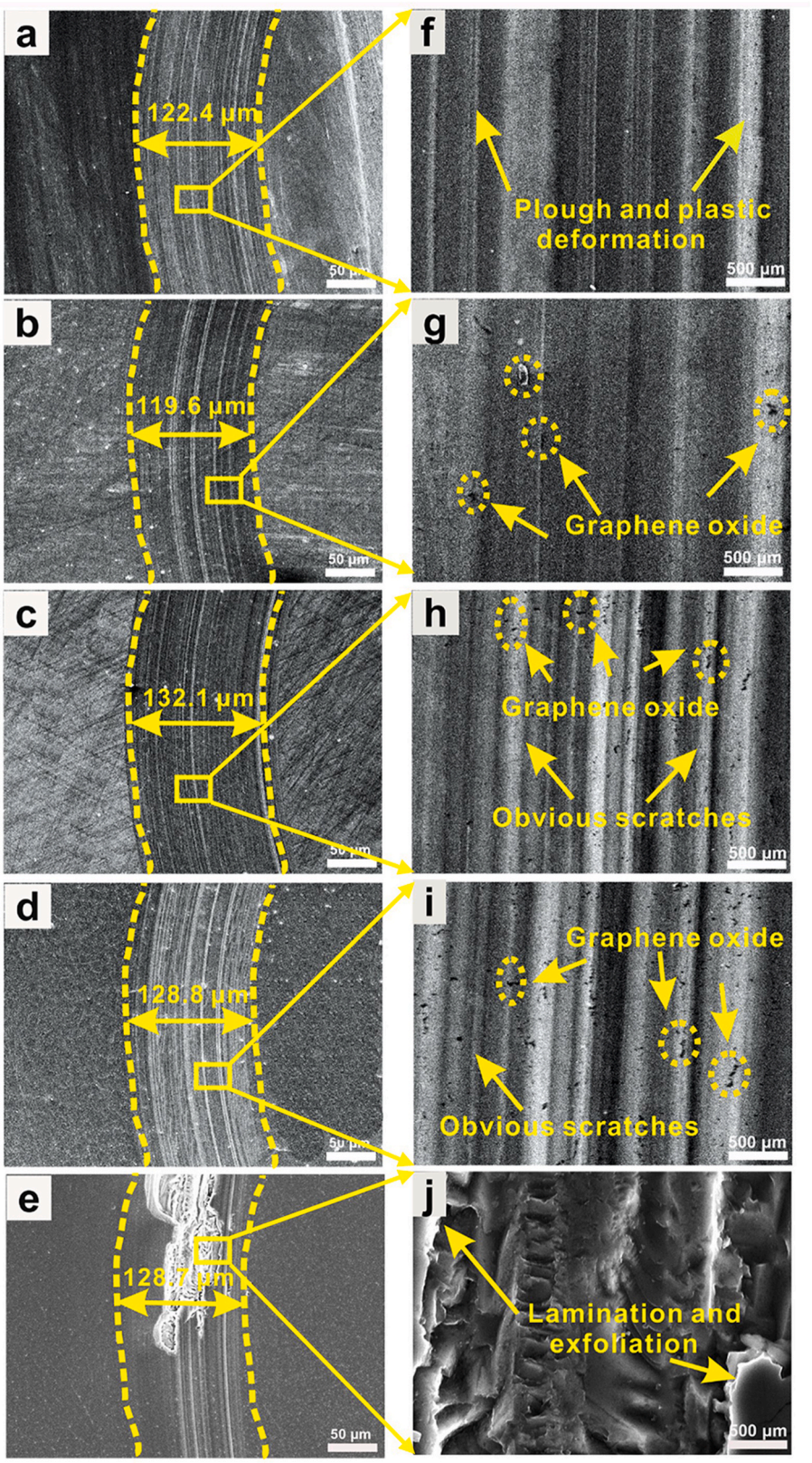

Fig. 8. Wear tracks and their enlarged views of Ti/Al-DLC films lubricated by (a)(f) pure oil (b)(g) PAO-GO1 (c)(h) PAO-GO2 (d)(i) PAO-GO3, and (e)(j) PAO-GO4, respectively, after sliding processes.

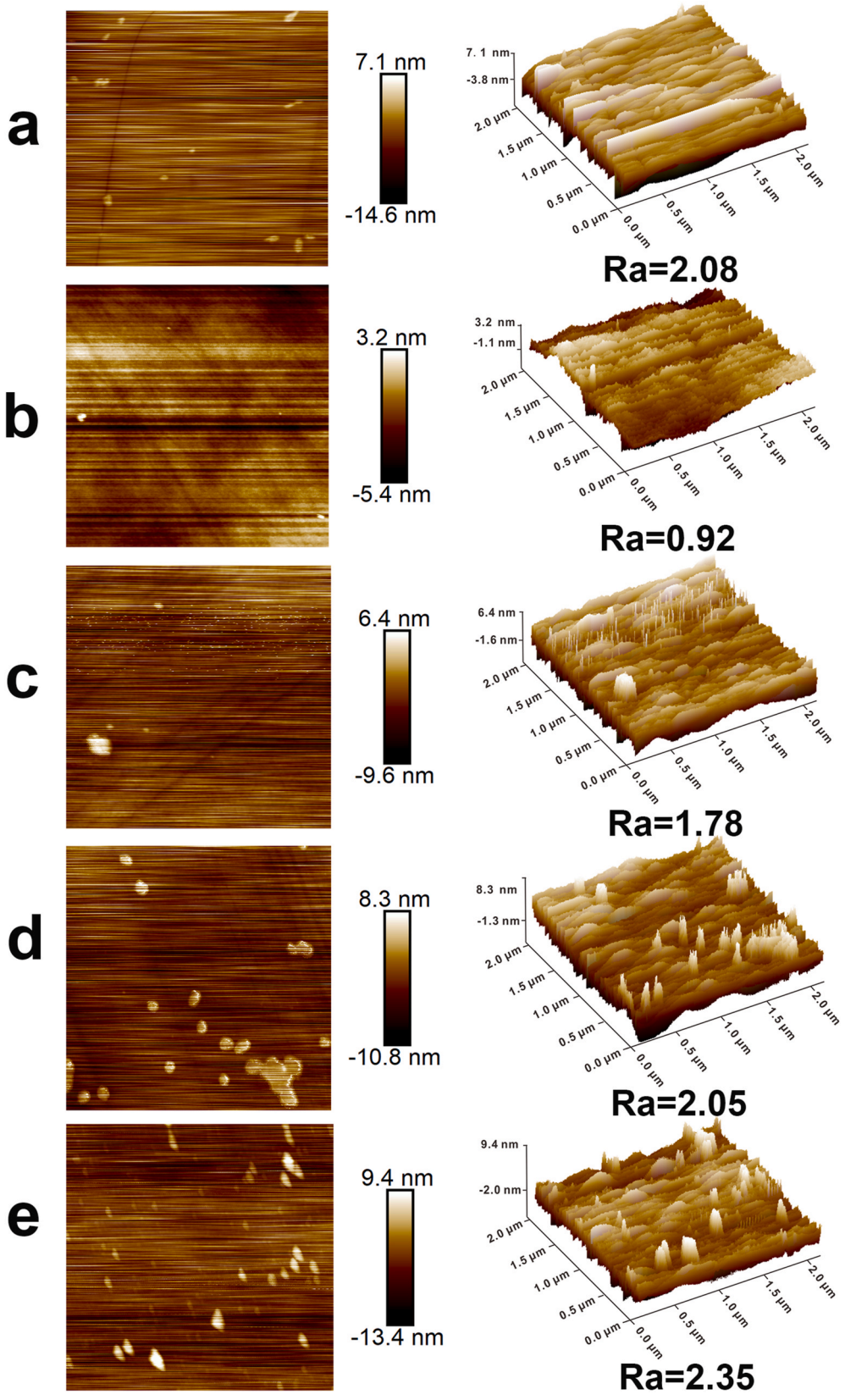

Fig. 9. AFM semicontact images of the wear tracks of Ti/Al-DLC films lubricated by (a) Pure oil, (b) PAO-GO1, (c) PAO-GO2, (d)PAO-GO3, and (e) PAO-GO4, respectively, after sliding processes.

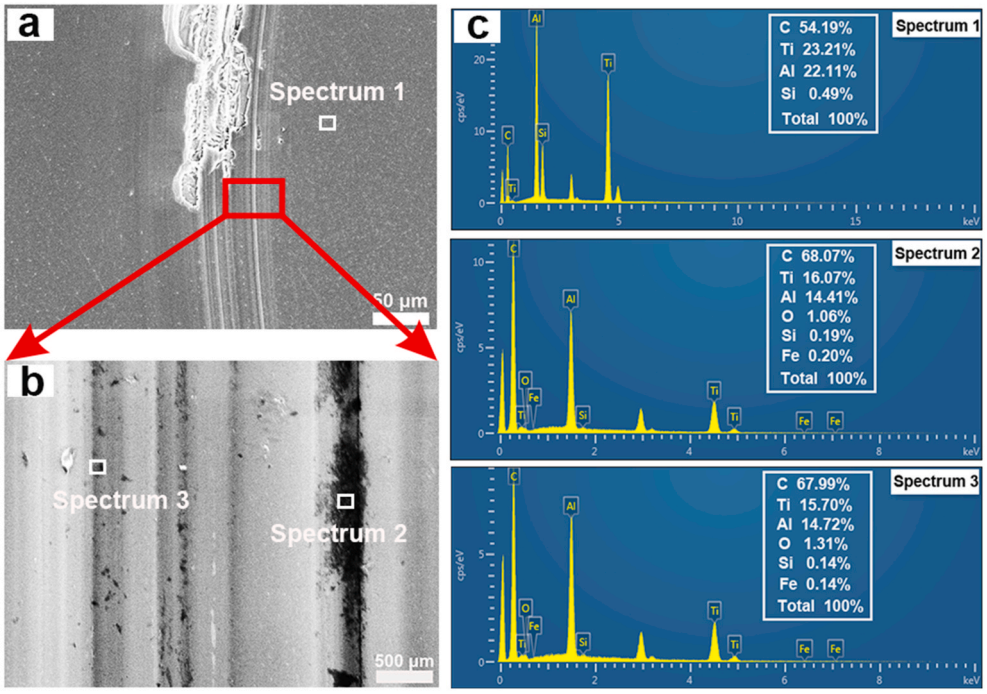

Fig. 10. (a–b) SEM micrographs and (c) EDS spectra of wear track for Ti/Al-DLC film lubricated by 0.018 wt% of GO composite oil.

trends as the GO concentration in PAO oil further increases to 0.018 wt% (Fig. 7) following the presence of many deep ploughs in the wear scars (Fig. 6). These results agree well with the wear rate of the film, as illustrated in Fig. 5.

3.4. Tribological mechanism

Because no obvious transfer layer is observed in the mating balls (Fig. 6), we focus on the structural transformation of the wear track on the film to clarify the underlying friction and wear mechanisms induced

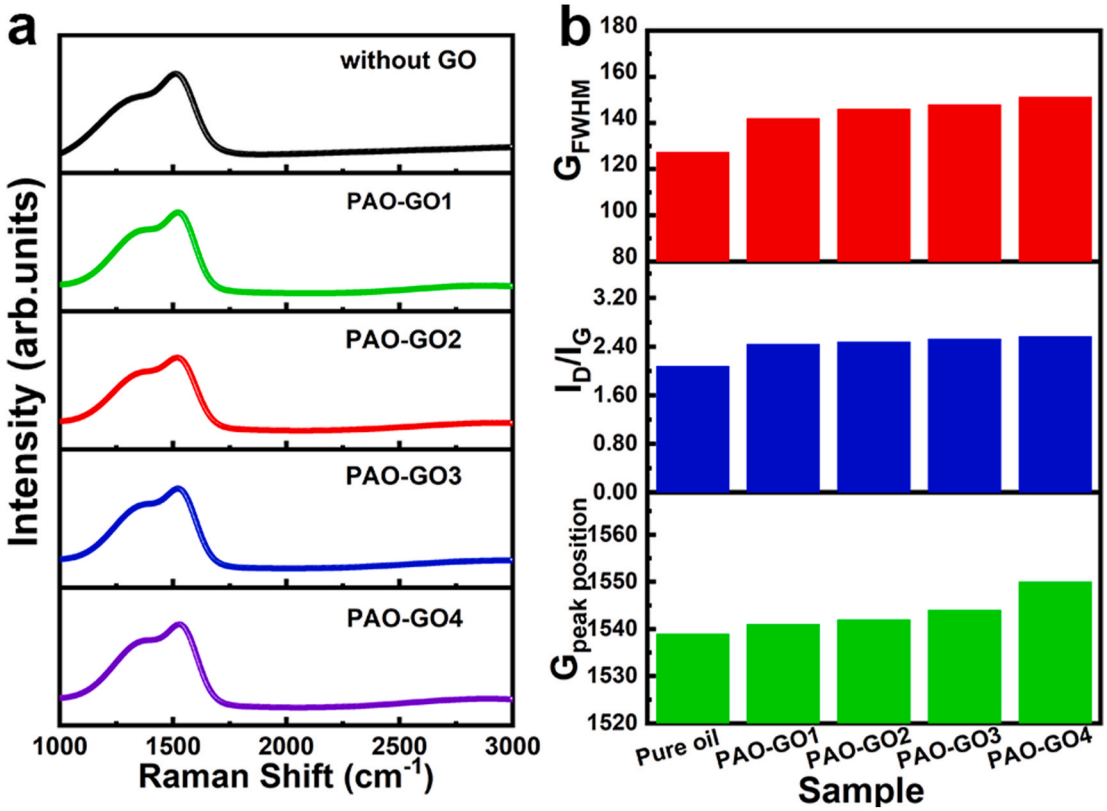

Fig. 11. (a) Raman spectra and (b) fitting results of the wear tracks of Ti/Al-DLC films lubricated by pure and GO-dispersed PAO oils, respectively.

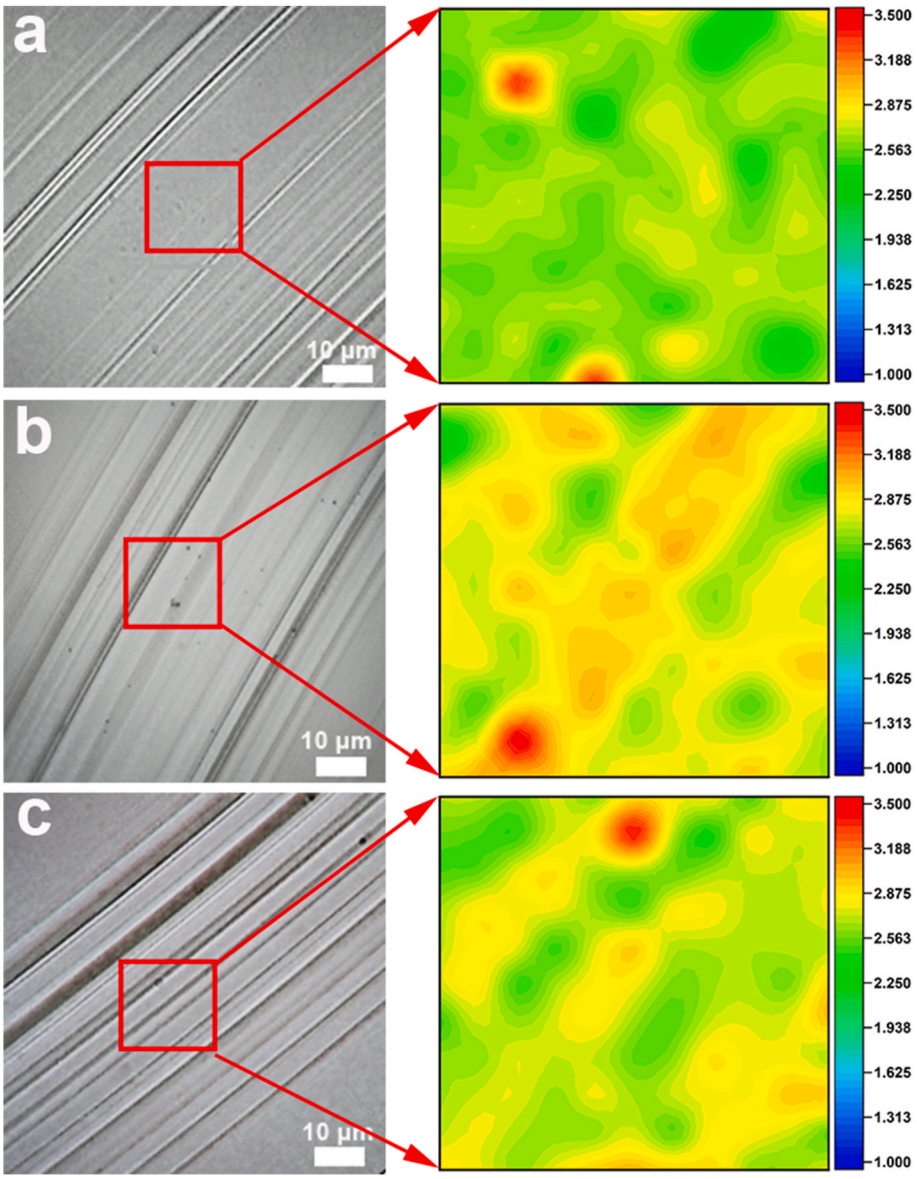

Fig. 12. Raman mappings of selected worn surfaces of films lubricated by (a) pure PAO oil, (b) PAO-GO1, and (c) PAO-GO4, respectively, in which color represents the different I_D/I_G values.

by different GO concentrations. Fig. 8 presents the wear profiles and their corresponding enlarged morphologies of Ti/Al-DLC films lubricated by pure and GO-dispersed PAO oils, respectively, after the sliding processes. For the pure oil case (Fig. 8(a) and (f)), the width of the wear track is 122.4 μm and some shallow furrows exist inside the wear track, accompanied by the plastic deformation of the worn surface [37], and the surface roughness of the wear track is approximately 2.08 nm (Fig. 9 (a)). As the GO additive is dispersed in PAO oil, the width and roughness of the wear track as a function of GO concentration first decrease and then increase. When lubricated by PAO-GO1, the width of the wear track reaches a minimum value of 119.6 μm (Fig. 8(b)); the worn surface is shallow and has the lowest surface roughness value (Ra = 0.92 nm Fig. 9 (b)) when compared to other lubricating conditions (Fig. 9). Besides, it can be noticed that some black particles adhere to the worn surface (Fig. 8(g)), which is related to the adsorption of GO additives and also indicates the presence of adhesive wear during the sliding process.

However, with further increase in the GO concentration to 0.006 wt % (PAO-GO2) and 0.012 wt% (PAO-GO3), both the width of wear track and dark particles inside the wear trace increase (Fig. 8 (c), (d), (h), and (i)), but some scratches and traces of deformation are visible on the surface, suggesting extra contribution from abrasive wear. In particular, there are obvious white bumps observed in Fig. 9(c) and (d), which originate from the aggregation of GO additives in the wear track [37]. This is consistent with the SEM analysis (Fig. 8). Furthermore, when the GO concentration reaches 0.018 wt% (Fig. 8(e) and (j)), partial delamination and exfoliation occur inside the wear track. It arises from the excess GO additive, causing aggregation and bonding between the GO sheets during the sliding process. This increases the interfacial roughness (2.35 nm, Fig. 9(e)), cross-links the mated surfaces, blocks the hydrodynamic lubrication of PAO oil, and hinders the sliding of tribopairs [38]. However, compared to the wear rate, the COF remains low without a significant increase (Fig. 4(b)). Therefore, we further explored the morphology and composition of the worn surface, as illustrated in Fig. 10. As shown in the enlarged view of the worn surface (Fig. 10(b)), the dark regions are noticeable on the rubbing surface. Further EDS analysis (Fig. 10(c)) reveals that compared to the as-deposited surface (spectrum 1), these dark areas (spectrums 2 and 3) exhibit an increased amount of carbon on the worn surface, which are attributed to the GO additives adsorbed to the surface [39,40]. Moreover, the adsorption of oil molecules in the worn region of the DLC surface plays a crucial role in

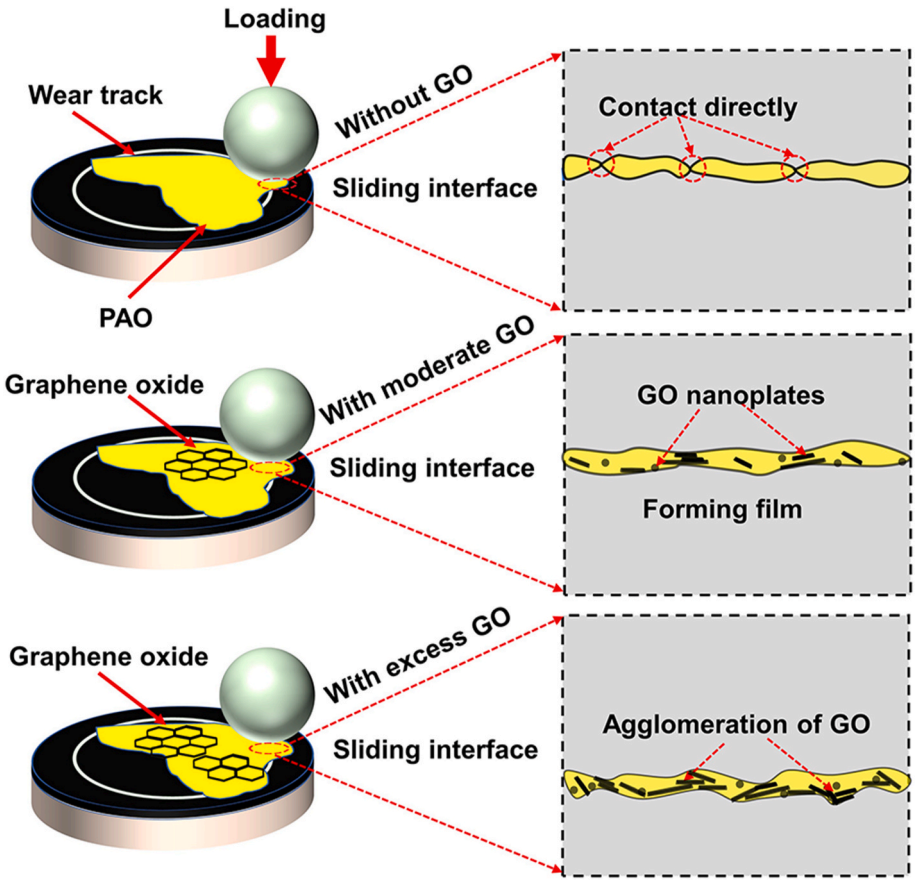

Fig. 13. Schematic of the GO-induced lubricating mechanism.

lowering the COF value and reducing the risk of DLC self-consumption in practical applications.

Fig. 11(a) shows the Raman spectra of the wear tracks of Ti/Al-DLC films lubricated by pure and GO-dispersed PAO oils. The quantitative fitting results are shown in Fig. 11(b). As the GO concentration increases from 0 to 0.018 wt%, the contribution of GO to the spectrum gradually increases, as evidenced by the increased D band intensity (Fig. 11(a)). However, the intensity ratio of the D band to G band as a function of GO concentration shows slight change. In addition, the blue shift of the G band is correlative with the average size of sp^2 domains. This is because the GO easily tears under Hertz contact stress, resulting in disordered GO with a significantly small size [21,41]. These results confirm that the carbon content is increased, as measured with the EDS analysis (Fig. 10 (c)).

Raman mappings inside the worn surfaces with sizes of 20 μm × 20 μm were further conducted, as shown in Fig. 12, to disclose the effect of the GO additive on the friction of the Ti/Al-DLC film. The color bar corresponds to different I_D/I_G values at the selected worn area. As can be observed, compared to lubrication by pure PAO oil only (Fig. 12(a)), when the GO concentration in PAO oil is 0.003 wt%, a high I_D/I_G value is obtained, suggesting the enhanced graphitization of the rubbing surface (Fig. 12(b)), which contributes to the antifriction behavior of the film. However, when GO concentration increases to 0.018 wt% (Fig. 12(c)), the excessively high concentration of GO can in turn suppress the triboinduced graphitization owing to the agglomeration of GO additive (Fig. 8) and the increased surface roughness (Fig. 9).

According to the aforementioned analysis, the GO-induced lubricating mechanism is illustrated in Fig. 13. When lubricated by pure PAO oil, direct contact between the GCr15 steel ball and Ti/Al-DLC film generates a high Hertz contact stress, causing the rapid collapse of the oil film. However, the addition of GO additives in PAO oil endowed the film with a sudden decrease in both the friction and wear rate owing to the interfacial graphitization (Fig. 12) and the adsorption of GO nanoplates on contacting surface (Fig. 8). Therefore, the roughness of the rubbing surface was reduced (Fig. 9(e)), smoothing the sliding interface and preventing the cold welding of the mated surfaces, which is also favorable for the hydrodynamic lubrication of PAO oil. However, at high GO concentrations, the homogeneous distribution of GO-dispersed PAO oil was disrupted, and the excess GO additive promoted serious agglomeration (Fig. 9). This caused the increased roughness (Fig. 7) and cross-linking of mating surfaces, aggravating the sliding resistance of both the mating surfaces and PAO oil.

4. Conclusion

In this work, Ti/Al-DLC films were fabricated on silicon substrates using an HIB system, and the effect of the concentration of GO as an additive on the tribological behavior of Ti/Al-DLC films under oil lubrication conditions was systematically explored. The results revealed that GO, as an additive of lubricating oil, played a significant role in enhancing the tribological performance of Ti/Al-DLC films. Compared to the case with pure PAO oil, when GO with concentration of 0.003 wt% was formulated into oil, the system achieved excellent friction reduction and wear resistance performances, decreased by 38.4% and 23.5%, respectively. However, when the GO concentration was further increased, it resulted in an increase in both the COF and wear rate. Microstructure analysis of the wear track indicated that at a low concentration (0.003 wt%), the GO could form a discontinuous and thin tribofilm to smooth the friction interface, and thus, prevent the direct contact between the friction pairs. Combined with the triboinduced graphitization, the shearing strength of the sliding interface was reduced, accounting for the improved antifriction and wear-resistance

behaviors. However, at high GO concentrations such as 0.018 wt%, the layered structure of GO was not retained owing to the serious agglomeration, which aggravated the interfacial roughness and cross-linking of mated surfaces. Additionally, the graphitization of friction interface was weakened, leading to the increased shearing barrier following the severe abrasive wear and high friction coefficient.

Declaration of competing interest

We declare that we have no financial and personal relationships with other people or organizations that can inappropriately influence our work, there is no professional or other personal interest of any nature or kind in any product, service and/or company that could be construed as influencing the position presented in, or the review of, the manuscript entitled.

Acknowledgments

This research was supported by the National Natural Science Foundation of China (51772307), National Science and Technology Major Project (2017-VII-0012-0108), A-class pilot of the Chinese Academy of Sciences (XDA22010303), Ningbo Science and Technology Innovation Project (2018B10014), the K. C. Wong Education Foundation (GJTD-2019-13), and the Korea Research Fellowship Program funded by the Ministry of Science and ICT through the National Research Foundation of Korea (2017H1D3A1A01055070).

Appendix A. Supplementary data

Supplementary data to this article can be found online at https://doi.org/10.1016/j.ceramint.2020.12.228.

References

[1] K. Holmberg, A. Erdemir, Influence of tribology on global energy consumption, costs and emissions, Friction 5 (2017) 263–284.
[2] S. Zhang, T. Ma, A. Erdemir, Q. Li, Tribology of two-dimensional materials: from mechanisms to modulating strategies, Mater. Today 26 (2019) 67–86.
[3] V.W. Wong, S.C. Tung, Overview of automotive engine friction and reduction trends-Effects of surface, material, and lubricant-additive technologies, Friction 4 (2016) 1–28.
[4] X. Dou, A.R. Koltonow, X. He, H.D. Jang, Q. Wang, Y.-W. Chung, J. Huang, Self-dispersed crumpled graphene balls in oil for friction and wear reduction, Proc. Natl. Acad. Sci. U. S. A 113 (2016) 1528–1533.
[5] X. Liu, L. Wang, Q. Xue, DLC-based solid–liquid synergetic lubricating coatings for improving tribological behavior of boundary lubricated surfaces under high vacuum condition, Wear 271 (2011) 889–898.
[6] L. Zhang, J. Pu, L. Wang, Q. Xue, Frictional dependence of graphene and carbon nanotube in diamond-like carbon/ionic liquids hybrid films in vacuum, Carbon 80 (2014) 734–745.
[7] X. Li, A. Wang, K.-R. Lee, Mechanism of contact pressure-induced friction at the amorphous carbon/alpha olefin interface, npj Computational Materials 4 (2018).
[8] D. Berman, A. Erdemir, A.V. Sumant, Graphene: a new emerging lubricant, Mater. Today 17 (2014) 31–42.
[9] A. Grill, Diamond-like carbon coatings as biocompatible materials—an overview, Diam. Relat. Mater. 12 (2003) 166–170.
[10] A. Choleridis, S. Sao-Joao, J. Ben-Mohamed, D. Chern, V. Barnier, G. Kermouche, C. Heau, M.-A. Leroy, J. Fontaine, S. Descartes, C. Donnet, H. Klöcker, Experimental study of wear-induced delamination for DLC coated automotive components, Surf. Coating. Technol. 352 (2018) 549–560.
[11] P.F. Macário, A. Vieira, L. Manfroi, M.G.P. da Silva, P. Leite, L. Vieira, Corrosion behavior of Al2024-T3, Al5052-H32, and Al6061-T6 aluminum alloys coated with DLC films in aviation fuel medium, Jet A-1 and AVGAS 100LL, Materials and Corrosion 70 (2019) 2278–2291.
[12] S. Zhou, L. Wang, S.C. Wang, Q. Xue, Comparative study of simplex doped nc-WC/a-C and duplex doped nc-WC/a-C(Al) nanocomposite coatings, Appl. Surf. Sci. 257 (2011) 6971–6979.
[13] X. Li, P. Guo, L. Sun, A. Wang, P. Ke, Ab initio investigation on Cu/Cr codoped amorphous carbon nanocomposite films with giant residual stress reduction, ACS Appl. Mater. Interfaces 7 (2015) 27878–27884.
[14] X. Li, L. Sun, P. Guo, P. Ke, A. Wang, Structure and residual stress evolution of Ti/Al, Cr/Al or W/Al co-doped amorphous carbon nanocomposite films: insights from ab initio calculations, Mater. Des. 89 (2016) 1123–1129.
[15] L. Sun, P. Guo, P. Ke, X. Li, A. Wang, Synergistic effect of Cu/Cr co-doping on the wettability and mechanical properties of diamond-like carbon films, Diam. Relat. Mater. 68 (2016) 1–9.
[16] S.W. Liu, H.P. Wang, Q. Xu, T.B. Ma, G. Yu, C. Zhang, D. Geng, Z. Yu, S. Zhang, W. Wang, Y.Z. Hu, H. Wang, J. Luo, Robust microscale superlubricity under high contact pressure enabled by graphene-coated microsphere, Nat. Commun. 8 (2017) 14029.
[17] H. Xiao, S. Liu, 2D nanomaterials as lubricant additive: a review, Mater. Des. 135 (2017) 319–332.
[18] J. Zhao, J. Mao, Y. Li, Y. He, J. Luo, Friction-induced nano-structural evolution of graphene as a lubrication additive, Appl. Surf. Sci. 434 (2018) 21–27.
[19] W. Zhang, M. Zhou, H. Zhu, Y. Tian, K. Wang, J. Wei, F. Ji, X. Li, Z. Li, P. Zhang, D. Wu, Tribological properties of oleic acid-modified graphene as lubricant oil additives, J. Phys. Appl. Phys. 44 (2011) 205303.
[20] V. Eswaraiah, V. Sankaranarayanan, S. Ramaprabhu, Graphene-based engine oil nanofluids for tribological applications, ACS Appl. Mater. Interfaces 3 (2011) 4221–4227.
[21] L. Wu, L. Gu, Z. Xie, C. Zhang, B. Song, Improved tribological properties of Si3N4/GCr15 sliding pairs with few layer graphene as oil additives, Ceram. Int. 43 (2017) 14218–14224.
[22] Z.-L. Cheng, W. Li, P.-R. Wu, Z. Liu, Study on structure-activity relationship between size and tribological properties of graphene oxide nanosheets in oil, J. Alloys Compd. 722 (2017) 778–784.
[23] T. Guo, C. Kong, X. Li, P. Guo, Z. Wang, A. Wang, Microstructure and mechanical properties of Ti/Al co-doped DLC films: dependence on sputtering current, source gas, and substrate bias, Appl. Surf. Sci. 410 (2017) 51–59.
[24] X. Li, P. Guo, L. Sun, X. Zuo, D. Zhang, P. Ke, A. Wang, Ti/Al co-doping induced residual stress reduction and bond structure evolution of amorphous carbon films: an experimental and ab initio study, Carbon 111 (2017) 467–475.
[25] C. Kong, P. Guo, L. Sun, Y. Zhou, Y. Liang, X. Li, P. Ke, K.-R. Lee, A. Wang, Tribological mechanism of diamond-like carbon films induced by Ti/Al co-doping, Surf. Coating. Technol. 342 (2018) 167–177.
[26] Y. Zhou, P. Guo, L. Sun, L. Liu, X. Xu, W. Li, X. Li, K.-R. Lee, A. Wang, Microstructure and property evolution of diamond-like carbon films co-doped by Al and Ti with different ratios, Surf. Coating. Technol. 361 (2019) 83–90.
[27] X. Xu, P. Guo, L.C.O. Tiong, X. Zuo, X. Li, K.-R. Lee, P. Cui, P. Ke, A. Wang, Role of dimple textured surface on tribological properties of Ti/Al-codoped diamond-like carbon films, Thin Solid Films 708 (2020) 138136.
[28] S. Singh, X. Chen, C. Zhang, R. Tyagi, J. Luo, Investigation on the lubrication potential of graphene oxide aqueous dispersion for self-mated stainless steel tribo-pair, Vacuum 166 (2019) 307–315.
[29] L. Wu, Z. Xie, L. Gu, B. Song, L. Wang, Investigation of the tribological behavior of graphene oxide nanoplates as lubricant additives for ceramic/steel contact, Tribol. Int. 128 (2018) 113–120.
[30] H. Kinoshita, Y. Nishina, A.A. Alias, M. Fujii, Tribological properties of monolayer graphene oxide sheets as water-based lubricant additives, Carbon 66 (2014) 720–723.
[31] J. Chen, Y. Zhang, M. Zhang, B. Yao, Y. Li, L. Huang, C. Li, G. Shi, Water-enhanced oxidation of graphite to graphene oxide with controlled species of oxygenated groups, Chem. Sci. 7 (2016) 1874–1881.
[32] R. Gusain, O.P. Khatri, Ultrasound assisted shape regulation of CuO nanorods in ionic liquids and their use as energy efficient lubricant additives, J. Mater. Chem. 1 (2013) 5612–5619.
[33] S. Eigler, C. Dotzer, A. Hirsch, M. Enzelberger, P. Müller, Formation and decomposition of CO2 intercalated graphene oxide, Chem. Mater. 24 (2012) 1276–1282.
[34] C. Wang, L. Feng, H. Yang, G. Xin, W. Li, J. Zheng, W. Tian, X. Li, Graphene oxide stabilized polyethylene glycol for heat storage, Phys. Chem. Chem. Phys. 14 (2012) 13233–13238.
[35] M. Gajendiran, S.M. Jainuddin Yousuf, V. Elangovan, S. Balasubramanian, Gold nanoparticle conjugated PLGA-PEG-SA-PEG-PLGA multiblock copolymer nanoparticles: synthesis, characterization, in vivo release of rifampicin, J. Mater. Chem. B 2 (2014) 418–427.
[36] B. Gupta, N. Kumar, K. Panda, S. Dash, A.K. Tyagi, Energy efficient reduced graphene oxide additives: mechanism of effective lubrication and antiwear properties, Sci. Rep. 6 (2016) 18372.
[37] A.A. Novikova, V.E. Burlakova, V.N. Varavka, I.E. Uflyand, E.G. Drogan, V. A. Irkha, Influence of glycerol dispersions of graphene oxide on the friction of rough steel surfaces, J. Mol. Liq. 284 (2019) 1–11.
[38] O. Elomaa, V.K. Singh, A. Iyer, T.J. Hakala, J. Koskinen, Graphene oxide in water lubrication on diamond-like carbon vs. stainless steel high-load contacts, Diam. Relat. Mater. 52 (2015) 43–48.
[39] Y. Ye, C. Wang, Y. Wang, W. Zhao, J. Li, Y. Yao, A novel strategy to enhance the tribological properties of Cr/GLC films in seawater by surface texturing, Surf. Coating. Technol. 280 (2015) 338–346.
[40] D. He, S. Zheng, J. Pu, G. Zhang, L. Hu, Improving tribological properties of titanium alloys by combining laser surface texturing and diamond-like carbon film, Tribol. Int. 82 (2015) 20–27.
[41] A.C. Ferrari, S.E. Rodil, J. Robertson, Interpretation of infrared and Raman spectra of amorphous carbon nitrides, Phys. Rev. B 67 (2003) 155306.